

UNIVERSITY OF BIRMINGHAM

Research at Birmingham

A local-global coupled-layer puppet model for robust online human pose tracking

Ma, Miao; Marturi, Naresh; Li, Yibin; Stolkin, Rustam; Leonardis, Ales

DOI:

[10.1016/j.cviu.2016.08.010](https://doi.org/10.1016/j.cviu.2016.08.010)

License:

Creative Commons: Attribution-NonCommercial-NoDerivs (CC BY-NC-ND)

Document Version

Peer reviewed version

Citation for published version (Harvard):

Ma, M, Marturi, N, Li, Y, Stolkin, R & Leonardis, A 2016, 'A local-global coupled-layer puppet model for robust online human pose tracking', *Computer Vision and Image Understanding*.
<https://doi.org/10.1016/j.cviu.2016.08.010>

[Link to publication on Research at Birmingham portal](#)

Publisher Rights Statement:

Checked 11/10/2016

General rights

Unless a licence is specified above, all rights (including copyright and moral rights) in this document are retained by the authors and/or the copyright holders. The express permission of the copyright holder must be obtained for any use of this material other than for purposes permitted by law.

- Users may freely distribute the URL that is used to identify this publication.
- Users may download and/or print one copy of the publication from the University of Birmingham research portal for the purpose of private study or non-commercial research.
- User may use extracts from the document in line with the concept of 'fair dealing' under the Copyright, Designs and Patents Act 1988 (?)
- Users may not further distribute the material nor use it for the purposes of commercial gain.

Where a licence is displayed above, please note the terms and conditions of the licence govern your use of this document.

When citing, please reference the published version.

Take down policy

While the University of Birmingham exercises care and attention in making items available there are rare occasions when an item has been uploaded in error or has been deemed to be commercially or otherwise sensitive.

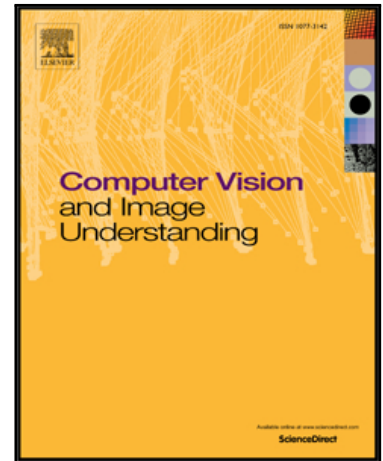
If you believe that this is the case for this document, please contact UBIRA@lists.bham.ac.uk providing details and we will remove access to the work immediately and investigate.

Accepted Manuscript

A Local-Global Coupled-Layer Puppet Model for Robust Online Human Pose Tracking

Miao Ma, Naresh Marturi, Yibin Li, Rustam Stolkin, Ales Leonardis

PII: S1077-3142(16)30118-7
DOI: [10.1016/j.cviu.2016.08.010](https://doi.org/10.1016/j.cviu.2016.08.010)
Reference: YCVIU 2473



To appear in: *Computer Vision and Image Understanding*

Received date: 31 August 2015
Revised date: 28 May 2016
Accepted date: 22 August 2016

Please cite this article as: Miao Ma, Naresh Marturi, Yibin Li, Rustam Stolkin, Ales Leonardis, A Local-Global Coupled-Layer Puppet Model for Robust Online Human Pose Tracking, *Computer Vision and Image Understanding* (2016), doi: [10.1016/j.cviu.2016.08.010](https://doi.org/10.1016/j.cviu.2016.08.010)

This is a PDF file of an unedited manuscript that has been accepted for publication. As a service to our customers we are providing this early version of the manuscript. The manuscript will undergo copyediting, typesetting, and review of the resulting proof before it is published in its final form. Please note that during the production process errors may be discovered which could affect the content, and all legal disclaimers that apply to the journal pertain.

Highlights

- We propose a new method for online tracking of articulated human body poses.
- Our method offers online sequential tracking from one frame to the next.
- Many other methods mutually optimize poses offline over all frames of a sequence.
- We propose a novel cross-coupled global-local model of articulated human body pose.
- We propose an adaptive penalty function for optimizing the pose estimates.

A Local-Global Coupled-Layer Puppet Model for Robust Online Human Pose Tracking

Miao Ma^{a,b,*}, Naresh Marturi^{b,c}, Yibin Li^a, Rustam Stolkin^b, Ales Leonardis^b

^a*Shandong University, Jinan, Shandong, 250061, P.R.China*

^b*University of Birmingham, Edgbaston, Birmingham, B15 2TT, UK*

^c*KUKA robotics UK Ltd., Wednesbury Great Western Street, WS10 7LL, UK*

Abstract

This paper addresses the problem of online tracking of articulated human body poses in dynamic environments. Many previous approaches perform poorly in realistic applications: often future frames or entire sequences are used anti-causally to mutually refine the poses in each individual frame, making online tracking impossible; tracking often relies on strong assumptions about *e.g.* clothing styles, body-part colours and constraints on body-part motion ranges, limiting such algorithms to a particular dataset; the use of holistic feature models limits the ability of optimisation-based matching to distinguish between pose errors of different body parts. We overcome these problems by proposing a coupled-layer framework, which uses the previous notions of deformable structure (DS) puppet models. The underlying idea is to decompose the global pose candidate in any particular frame into several local parts to obtain a refined pose. We introduce an adaptive penalty with our model to improve the searching scope for a local part pose, and also to overcome the problem of using fixed constraints. Since the pose is computed using only current and previous frames, our method is suitable for online sequential tracking. We have carried out empirical experiments using three different public benchmark datasets, comparing two variants of our algorithm against four recent state-of-the-art (SOA) methods from the literature. The results suggest comparatively strong performance

*Corresponding author

Email address: mamiaosdu@hotmail.com (Miao Ma)

of our method, regardless of weaker constraints and fewer assumptions about the scene, and despite the fact that our algorithm is performing online sequential tracking, whereas the comparison methods perform mutual optimisation backwards and forwards over all frames of the entire video sequence.

Keywords: human pose tracking, human tracking, video tracking, pose estimation, coupled-layer model.

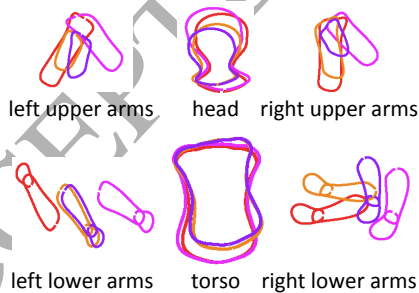
1. Introduction

Human pose estimation and tracking are increasingly popular research areas in computer vision, and have been studied for well over 30 years in the literature, *e.g.* [1]. There is growing interest in such algorithms for a variety of applications including activity recognition [2], video understanding [3], gesture analysis [4], human-robot interaction [5], and others. Significant advances were made in recent years, however even state-of-the-art (SOA) methods often rely on strong assumptions and constraints in representing human bodies, such as visual appearance [4], scale [6], lighting conditions, occlusions, and the ranges of motion of limbs and limb-parts. In this work, our goal is to sequentially track human body poses in monocular video frames obtained under variable conditions, where people move freely and interact with each other. Typical examples include videos of TV series or movies, where human appearance is unconstrained (*e.g.* variable background, any colour and type of clothing, no fixed scale, etc.). Many recent efforts have been devoted to track and estimate human poses from monocular video frames. Even though most of them perform well on certain body parts such as torsos and heads, their performance for arms is still not convincing. Within this context, we are most closely interested in tracking upper body poses, which include head, torso and arms, and in particular, improving the pose accuracy of lower arms. Nevertheless, our approach is not constrained for human upper body and can be easily adapted to the entire body. Our method is initialised from a single frame, and does not require any prior knowledge of the human clothing style, background scene or other conditions.

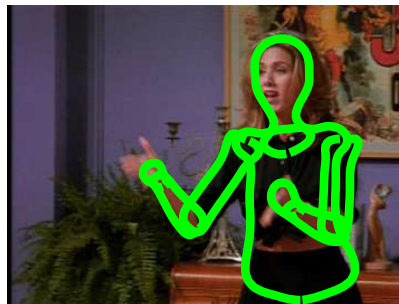
24 A variety of methods have been proposed in recent years to track and es-
 25 timate the poses of articulated human bodies. However, many methods make
 26 use of the entire image sequence to mutually refine the poses in each individual
 27 frame, *e.g.* [7, 8], rendering them only suitable for offline applications. In con-
 28 trast, our method relies only on the previous frame information at any point in
 29 time, with computation only in the temporal direction, enabling online tracking
 30 applications. Since this reduction in available temporal information affects the
 31 overall performance, our method makes use of additional information from the
 32 spatial domain. For estimating articulated human pose, the overall informa-
 33 tion associated with the target makes the state space too large to compute. In
 34 this case, we exploit a local-global coupled-layer method, which uses the entire
 35 human body as a global layer and uses decomposed parts as a local layer (see
 36 Fig. 1). This type of methodology not only reduces the computational space
 and cost, but also improves the overall accuracy.



(a) Global candidates.



(b) Local candidates



(c) Refined human pose

Figure 1: Proposed coupled-layer model. (a) Different global pose candidates; (b) Local parts obtained by decomposing the global pose candidates. (c) Recomposed global pose.

38 In this paper, we present an on-line coupled-layer method using discrete-
39 structure puppets [9] for estimating the upper human body pose information.
40 Recently published human pose estimation methods predominantly use an eval-
41 uation function to evaluate a candidate pose for the entire human body [10, 11].
42 However, such methods can become prone to local convergence problems. For
43 example, if one candidate pose suggests a correct left arm position, and an
44 erroneous right arm position, and an alternative candidate pose is vice versa,
45 then both candidates may generate similar evaluation scores. In this paper, we
46 address this problem by decomposing the entire body into smaller parts and
47 by estimating the pose separately for each of them. Nevertheless, if enough
48 constraints are not provided, this decomposition method will also be unreli-
49 able, *e.g.* left and right arms may erroneously swap places and converge on each
50 other’s true image locations. To resolve this issue we introduce an adaptive
51 penalty policy (Sec. 4.3.3) with our coupled-layer method to improve the scope
52 of local parts pose searching. It also assists in tackling variable body scales and
53 tuning any propagated erroneous poses.

54 The remainder of this paper is organized as follows. The methods that are
55 closely related to our work are presented in section 2. The proposed coupled-
56 layer model is presented in section 3, where we detail the model and explain
57 the relationship between its local and global layers. Section 4 explains the
58 tracking and estimation procedure, using the coupled-layer model. Section 5
59 presents experiments conducted using three different public benchmark datasets,
60 where we compare the performance of our method against four other SOA pose
61 estimation techniques. In this section, we also investigate the robustness of our
62 method to various different levels of initialization error. Section 6 concludes the
63 paper and the proposed method.

64 2. Related Work

65 Numerous human pose estimation techniques, developed for a variety of
66 applications, are available in the literature. In this section, we discuss the work

67 most closely related to our proposed method.

68 The well-known *pictorial structures* (PS) model, proposed by Fischler and
 69 Elschlager [12] in 1973, is still drawing significant attention from researchers for
 70 its efficient tree-based inference algorithm [11, 10, 13, 14, 15]. A key limitation
 71 of PS, and some extended models, is that the parts are treated as rigid templates
 72 and are represented as rectangular (or polygonal) regions. Later methods, such
 73 as *contour people* [16] and *deformable structures* (DS) model [9], that are de-
 74 rived from 3D human models, can better capture the 2D shape as non-rigid,
 75 deformable parts. However, due to the holistic nature of these models, several
 76 problems can arise e.g. in the case of rapid part motions or occlusions.

77 Several methods from the literature use some kind of hierarchical method-
 78 ology or coarse-to-fine scheme for inference. For example, Wu and Huang [17]
 79 used a two-layer model for hand motion tracking, where the palm motion is
 80 represented in the global model and the fingers motion in the local model. Kuo
 81 *et al.* [18] used a two-layer model which searches for the coarse location of the
 82 human body regions over the image sequence in one layer, and then estimates
 83 and refines detailed human body part poses over the image sequence in another
 84 layer. Lee and Nevatia [19] proposed a three-layer model. An alternative strat-
 85 egy is to model each part separately [20, 21, 22] and impose different constrains
 86 on different parts [23]. However, these methods estimate and evaluate the en-
 87 tire body together. Related works such as [24] and [7] focus on individual body
 88 parts *i.e.* to treat a single lower arm or an entire limb as an independent part to
 89 explore a set of poses. However, in such work, the entire video sequence is typi-
 90 cally used to mutually refine the poses over all images, making them unsuitable
 91 for online tracking. In contrast, in this paper we propose a local-global coupled
 92 strategy, in which poses are tracked in an online fashion from one frame to the
 93 next using a holistic body model for the global layer (Fig. 1(a)), while refining
 94 poses within each frame using individual body part models as the local layer
 95 (Fig. 1(b)).

96 In some pose estimation methods, optical flow information is exploited as
 97 a cue, either for body part detection or for frame-to-frame pose propagation.

98 Zuffi *et al.* [8] use both forwards and backwards optical flow to propagate pose.
99 The major drawback of this approach is that it cannot be used for online track-
100 ing. Additionally, the accuracy of such methods is limited unless applied to a
101 particular dataset, because the joint angle space is pre-constrained to match the
102 limited range of poses appearing in a particular video sequence. This makes the
103 method difficult to adapt to more varied datasets, or real world applications with
104 changing or uncertain scenes. Fragkiadaki *et al.* [25] have used kinematically
105 constrained optical flow for segmenting body parts and for propagating segmen-
106 tations over time. Cherian *et al.* [7] made use of the optical flow between current
107 and future frames to create loops for passing messages. The messages passed
108 within these loops then help to constrain the location of each node. Similar to
109 these methods, we also use optical flow in this work for both pose estimation
110 and propagation. However, we additionally exploit an adaptive penalty policy
111 which automatically constrains the searching space instead of fixing it in ad-
112 vance (particular to a given dataset) or using future information (offline mutual
113 refining of poses over all frames of a sequence).

114 Sometimes occlusions and self-occlusions occur in unconstrained environ-
115 ments, and such situations are difficult to handle. In 3D tracking, Cho *et al.* [26]
116 solved this problem by modeling self-occlusion states between two body parts
117 utilizing the 3D pose information of each body part (modeled as 3D cylinders).
118 However in 2D conditions, it is much harder to obtain depth information for
119 helping to detect occlusion states. Chen and Yuille [27] indirectly solved this
120 problem using an image dependent pairwise relational term for adjacent body
121 parts. In contrast, our work proposes an adaptive penalty policy, which makes
122 it possible to predict the possible location of a body part under occlusion, and
123 also enables the re-detection and tracking of the body part when it re-appears
124 following a period of occlusion.

125 A common schema for human pose estimation is, firstly, generating a number
126 of pose candidates, then constructing a reliable cost function as well as making
127 a non-maximum suppression (NMS) method to find the most likely human pose.
128 Sigal and Black [28] used a hierarchical method which need enough plausible

129 pose part candidates for belief propagation. Park and Ramanan [15] proposed a
 130 method to generate a diverse set of N-best candidate poses with small overlaps
 131 for a still image, depending on a large number of pose hypotheses generated
 132 using the method of [29]. Later, Cherian [7] decomposed the N-best candidates
 133 generated by [15] and recomposed them using information from all frames of
 134 the entire video sequence to find refined poses. Burgos *et al.* [30] define a
 135 loss function for the large number of predicted pose candidates, with respect
 136 to time and space for all frames of the entire sequence, and use the scores of
 137 the loss function to decide a final pose for each frame. In the work of Zuffi
 138 *et al.* [8], the NMS method is also used to generate a good initial estimate
 139 among numerous pose candidates for each still image. In this schema, the
 140 NMS method relies on information derived from all frames of the entire video
 141 sequence, which limits these methods only for offline applications, and also
 142 requires that the set of candidate poses is large enough to contain “good” poses
 143 for each frame. In contrast, our method does not rely on large numbers of extra
 144 pose candidates generated for each image. We only use a small number of whole
 145 body candidates in our global layer, and after decomposing global candidates
 146 into local candidates, our method is able to relocate keypoints to get additional
 147 local candidates and refine them online using only information from only the
 148 current frame and one previous frame.

149 3. Proposed Coupled-Layer Model using DS Puppets

150 The DS (deformable structures) puppet model is a 2D articulated human
 151 body model recently introduced by Zuffi *et al.* [9], and applied to human pose
 152 tracking and estimation in [8]. The human’s shape is expressed as a factored
 153 probability over parts [9]. The DS puppets model is learned from training con-
 154 tours derived from SCAPE [31] (Shape Completion and Animation of People),
 155 which is a parametric 3D model of articulated human shape. Our method is also
 156 based on the DS puppet, however, we decompose it into multiple layers (local
 157 and global) for estimating the final pose. Hence, we call our model a *coupled-*

158 *layer DS puppet model*. In our case, we use the model that has been trained
 159 using SCAPE while the testing is performed using SOA datasets explained in
 160 detail in Sec.5.1. The performed experiments point towards the generality and
 161 independence of the model.

162 Our coupled-layer model is inspired by the *local-global tracker* (LGT) [32],
 163 where a single target object, defined by a simple bounding box, is tracked by
 164 combining feature models (*e.g.* colour histograms, motions and shapes) for the
 165 overall object (global layer) and several small patches (the local layer). Each
 166 layer is used to help constrain (and thereby robustify) updates for the other
 167 layer. Our proposed articulated pose estimation method adopts a similar phi-
 168 losophy. As shown in Fig. 1, for a certain frame t , our method operates in
 169 three successive stages: procure global layer puppet, handle individual local
 170 layer parts and estimate refined global pose. The local layer contains groups of
 171 every upper body part and each group is comprised of several pose candidates.
 172 The process to initialise and select best pose candidates is detailed in Sec. 4.
 173 The global layer has nine keypoints to generate the entire human upper body,
 174 and in the similar fashion to local layer it has its own global pose candidates. In
 175 each frame, the entire global upper body poses are decomposed into local body
 176 parts, from which the local layer refines each part separately and filters out bad
 177 candidates. The refined local parts are re-combined into global layer candidates
 178 for further processing within the global layer.

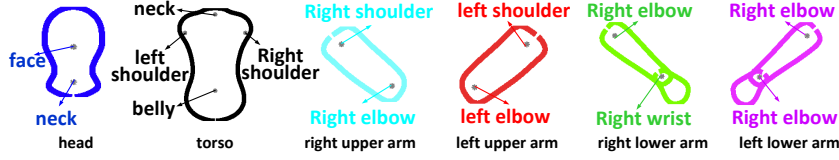
179 In Sec. 3.1 and Sec. 3.2 we describe the composition of local and global
 180 layers, respectively and in Sec. 3.3 we provide an overview of the local-global
 181 coupled-layer puppet model.

182 3.1. Local Layer

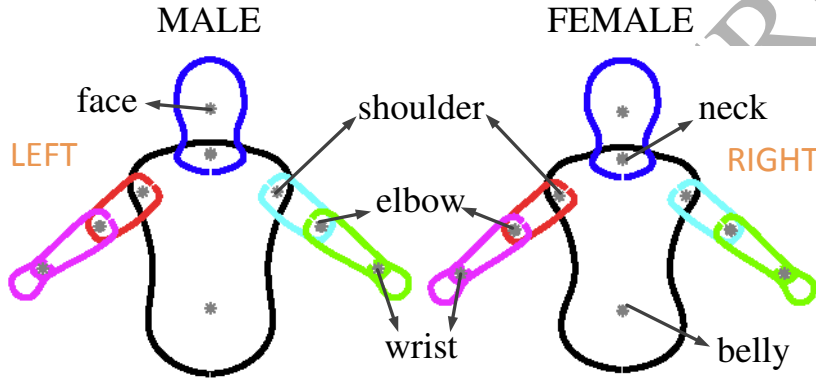
183 The local layer \mathcal{L} in the t^{th} frame is composed of 6 parts as follows:

$$\mathcal{L}_t = \{H_t, T_t, UA_t^r, UA_t^l, LA_t^r, LA_t^l\}, \quad (1)$$

184 where, H and T denote head and torso, UA^r and UA^l stand for right and left
 185 upper arms, LA^r and LA^l represent right and left lower arms, respectively (see



(a) Local parts with their keypoints $\mathbf{k}_i^{(j)}$, described in Eq.(2). For torso, $\mathbf{k}_i^{(j)}$ includes four keypoints while for other parts, $\mathbf{k}_i^{(j)}$ includes two keypoints.



(b) Global poses with their keypoints

Figure 2: Illustration of the keypoints in local and global layers. (a) Keypoints of each part present in the local layer of a female puppet. (b) Keypoint locations of the global upper body male and female puppets. It can be seen that every part has two keypoints, some of them also belong to other parts (e.g. neck, left/right elbows).

186 Fig. 1(b)). These six parts are the main body parts of the upper human body
 187 and contain vital human body pose information. For simplicity and sequential
 188 calculation, hereafter we maintain the same order for parts given in Eq.(1)
 189 throughout this work. Each individual part P_i ($i = 1 \cdots 6$ with 1 for head, 2 for
 190 torso and so on as in Eq.(1)) is specified by three elements:

$$P_i = \{\mathbf{k}_i^{(j)}, s_i^{(j)}, model_i\}_{j=1:N_i}, \quad (2)$$

191 where, N_i is the number of candidates of part i , $\mathbf{k}_i^{(j)}$ is the keypoints location
 192 of the j^{th} candidate in part i , see Fig. 2(a). For torso, $\mathbf{k}_i^{(j)}$ includes four key-
 193 points while for other parts, $\mathbf{k}_i^{(j)}$ includes two keypoints. $s_i^{(j)}$ is the scale of this

194 local layer candidate, which is inherited from the *scale* of global layer (scale
 195 computation is demonstrated in Sec. 3.2 and illustrated in Fig. 3) and $model_i$
 196 is the model of part i used to calculate the part candidate closed contour $\mathcal{C}_i^{(j)}$.
 197 This model has been obtained through the principal component analysis (PCA)-
 198 based method proposed by [9]. It contains a vector \mathbf{m}_i representing the mean
 199 contour and keypoints of part i , and a matrix \mathbf{B}_i containing the eigenvectors
 200 of the training data corresponding to the dominant eigenvalues, for each gender
 201 separately. For the reason that females and males require different models, the
 202 principal components are trained separately for both genders.

203 The relationship among $\mathbf{k}_i^{(j)}$, $s_i^{(j)}$, $\mathcal{C}_i^{(j)}$ and $model_i$ is shown in Eq.(3):

$$\begin{bmatrix} \mathcal{C}_i^{(j)} \\ \mathbf{k}_i^{(j)}, s_i^{(j)} \end{bmatrix} = \mathbf{B}_i \mathbf{z}_i^{(j)} + \mathbf{m}_i, \quad (3)$$

204 where, \mathbf{z}_i is a vector of linear shape coefficient. Given $\mathbf{k}_i^{(j)}$ and $s_i^{(j)}$, we can
 205 calculate $\mathbf{z}_i^{(j)}$ according to Eq.(3). With fixed $\mathbf{z}_i^{(j)}$, the contour $\mathcal{C}_i^{(j)}$ of the j^{th}
 206 local candidate can be calculated.

207 3.2. Global Layer

208 The global layer \mathcal{G} is able to estimate the shape and scale of the entire upper
 209 body and to connect the selected candidates of each part from the local layer in
 210 order to estimate the overall human body pose. Each global candidate in layer
 211 \mathcal{G} has 9 keypoints \mathcal{K} (shown in Fig. 2(b)) as follows:

$$\mathcal{K} = \{belly, face, neck, rsh, re, rw, lsh, le, lw\}, \quad (4)$$

212 where *rsh/lsh* mean right/left shoulders, *re/le* mean right/left elbows, and
 213 *rw/lw* mean right /left wrists. The global contour \mathcal{GC} of the q^{th} candidate in
 214 t^{th} frame is given by:

$$\mathcal{GC}_t^{(q)} = \bigcup_{i=\{i|i \subset \mathcal{L}_t\}} \mathcal{C}_i^{(q)}. \quad (5)$$

215 Each scale $s_i^{(q)}$ used to calculate $\mathcal{C}_i^{(q)}$ is of the same value with *scale*, which is
 216 described later in this section. Similar to the layer \mathcal{L} , different models for males

217 and females are used in this layer as shown in Fig. 2(b). Each global layer pose
 218 candidate has a probability $p(\mathbf{g}\mathbf{c}_t^{(q)}|\pi_{DS})$ according to the DS puppet defined
 219 in [8] (π_{DS} refers to DS model parameters), which represents the probability of
 220 a global model instance.

221 Here, we exploit a method to estimate the global model scale using defined
 222 keypoints \mathcal{K} . We find that the most invariant relative distance d_c of the key-
 223 points is:

$$d_c = d_{(neck,face)} + d_{(neck,lsh)} + d_{(neck,rsh)}. \quad (6)$$

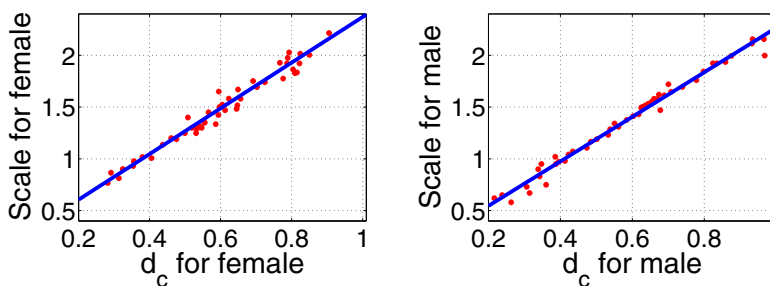
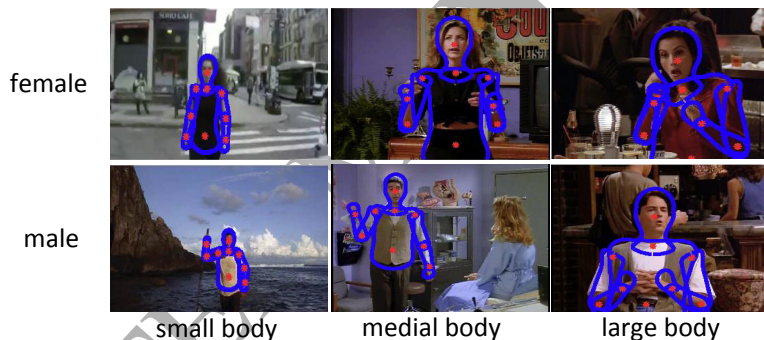
224 Eq. (6) gives the sum of the Euclidean distances between neck and head,
 225 and neck and left/right shoulders. In this context, we use “Transfer Learning”
 226 [33] to obtain a relationship between d_c and scale. This has been accomplished
 227 using 50 static images for each gender that are obtained from online image
 228 databases containing arbitrary human poses (with varying scale). For each
 229 image, we define a set of keypoints to calculate the d_c value (see Fig. 3(a)) and
 230 a corresponding scale value. Now, the obtained d_c and scale values will guide us
 231 in estimating a linear relationship as shown in Fig. 3(b). Since males and females
 232 require different body models, separate male and female sequences are used for
 233 training. Consequently, a global body puppet contour has been obtained in the
 234 first frame from Eq.(5) using nine keypoints, as shown in Fig. 3(c).

235 3.3. Overview of the Proposed Coupled-layer Model

236 A schematic overview of the proposed coupled-layer model is depicted in
 237 Fig. 4. In order to estimate the human body pose in frame $t + 1$, initially we
 238 propagate several best entire pose candidates estimated in frame t to frame $t + 1$
 239 according to optical flow (illustrated in Fig. 4 step1) which will be described in
 240 Sec. 4.2. Then we use a flexible mixtures of parts (FMP) method [10], which is
 241 a human pose estimation method for monocular still images, to generate several
 242 extra entire human pose candidates for frame $t + 1$ (Fig. 4 step2). This step is
 243 performed to provide more options when locating torsos. At this point, we have
 244 propagated candidates and initialised candidates (from FMP) in the global layer
 245 as shown in Fig. 1(a), and in the next step (Fig. 4 step3) we decompose them into



(a) Sample external images with pre-defined keypoints.

(b) Estimated linear relationship between scale and d_c .

(c) Suitable scale obtained from the relationship shown in (b).

Figure 3: (a) Sample images used for scale computation, first two show female body keypoints and the next two show male body keypoints. (b) and (c) Illustration of scale and global puppet estimation. (b) Relationship between d_c and scale, dots represent training samples. (c) Obtained initial frame global body puppets with different scales, dots represent keypoints.

246 local layer candidates (see Fig. 1(b)) for further processing. To refine these local
 247 layer candidates, we use a method described in Sec. 4.4 to generate additional
 248 relocated local part candidates when necessary (Fig. 4 step4). After this step, a
 249 cost function defined in Sec. 4.3 is used to select best local part candidates, which

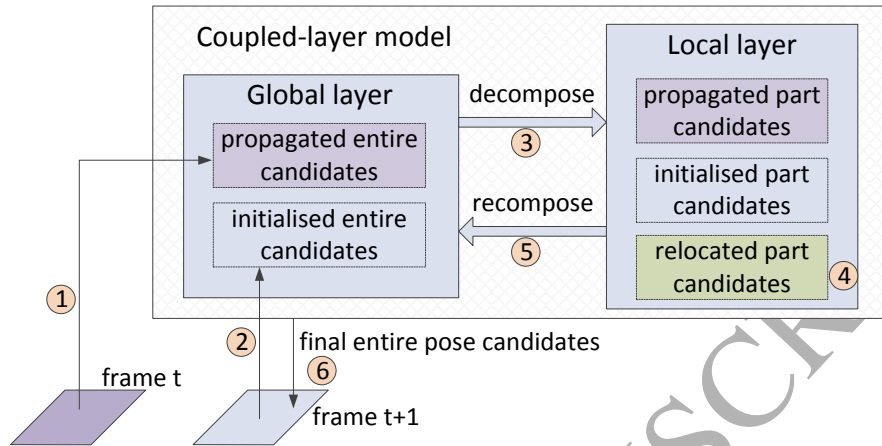


Figure 4: A schematic overview of *coupled-layer DS puppet model* for the frame $t + 1$. There are several steps: 1) propagate several best global human pose candidates from frame t to frame $t + 1$; 2) generate several entire pose candidates using FMP method for the frame $t + 1$; 3) decompose all the global layer candidates into local part candidates; 4) generate some relocated local part candidates when necessary; 5) recombine selected local parts into global candidates; 6) get final best entire human pose candidates for frame $t + 1$.

are later recombined into global entire human pose candidates (Fig. 4 step5).
 Then we evaluate the recombined global candidates (Sec. 4.1), and choose the
 best candidates to propagate to frame $t + 2$ for future pose estimation (Fig. 4
 step6). The best candidate is selected as the overall result of frame $t + 1$ (see
 Fig. 1(c)).

4. Inference

4.1. Body Pose Initialization

Our method does not use any posterior information (unlike [8] which uses
 forwards and backwards temporal propagation), and the available knowledge
 about each part is limited. To resolve this problem, some researchers have
 assumed prior knowledge such as the colour of the tracked person's clothes [8] or
 a predetermined start pose, and others, e.g. [34], assume a manual initialization
 at the first frame (similar to conventions of the mainstream target tracking

263 literature). In this work we follow the latter approach by defining the puppet
 264 manually in the first frame of the video sequence. This is accomplished by
 265 selecting nine keypoints of a human body (*e.g.* belly button, neck, face, etc.
 266 that are defined in Eq.(4)), and then Eq.(5) is used to obtain the initial global
 267 pose (Fig. 3(c)).

268 People often wear coloured clothes (either with long or short sleeves) and this
 269 colour information can be used for recognition and tracking. In our method,
 270 we extract colour histograms $h_c(i)$ for each local part i from the first frame,
 271 handling self-occlusion from lower arms to upper arms, and then to torso and
 272 head. The RGB image frames are transformed into the CIE L*a*b* colour space,
 273 and the pixels which have very small Lightness values ($L < 0.3$) are ignored.
 274 The two colour dimensions (a and b) and 20×20 bins are used to calculate
 275 the colour histograms $h_c(i)$. Later, this information is used for matching in the
 276 local layer (as presented in Sec. 4.3.1).

277 4.2. Global Layer Pose Tracking

278 Due to the possibility of erroneous hand-initialised poses (or, in future ap-
 279 plications, erroneous automatic detections) in the first frame, we perturb the
 280 initialised pose to obtain several global pose candidates. As discussed in Sec. 3.3,
 281 after processing each frame, we get several global pose candidates for propaga-
 282 tion. We calculate the score of each global layer candidate, based on which the
 283 best candidates for propagation are selected. In our method, the best 8 can-
 284 didates are selected for propagating to the next frame. The score for any q^{th}
 285 global candidate in the t^{th} frame is computed as follows:

$$score_t^{(q)} = \psi_t^{(q)} + \phi_t^{(q)} = \lambda_\psi p(I_t | \mathcal{GC}_t^{(q)}) + \lambda_\phi p(\mathcal{GC}_t^{(q)} | \pi_{DS}), \quad (7)$$

286 where the coefficients $\lambda_\psi \gg \lambda_\phi$ for the reason that the magnitude of $\phi_t^{(q)}$ is
 287 larger than $\psi_t^{(q)}$. The first term $\psi_t^{(q)} = p(I_t | \mathcal{GC}_t^{(q)})$ contains the image likelihood
 288 (*i.e.* colour and contour likelihood) for the entire puppet, I_t is the t^{th} frame of
 289 video sequence, and $\mathcal{GC}_t^{(q)}$ is the q^{th} whole puppet candidate contour for the
 290 current frame. The second term in Eq. (7), $\phi_t^{(q)}$ (defined in [8]) represents the

291 probability of a DS model instance. We assume that the set of best poses in
 292 frame t are approximately correct, and we then track the whole body poses from
 293 frame t to $t+1$ using the optical flow of each part region of frame t . The optical
 294 flow images are computed using the method proposed by Liu [35]. Next, we
 295 calculate an affine matrix $\mathbf{A}_i^{(q)}$ (an affine motion model proposed by [8]) for each
 296 individual part i within the candidate q , which is used to estimate displacements
 297 of keypoints \mathcal{K} . Because some keypoints may lie at the intersection region of two
 298 different parts, the final displacement for such keypoints is approximated by the
 299 mean of that found for each part. The keypoint displacements are calculated as

$$vp_k^{(q)} = \frac{1}{N_k} \sum_{i=\{i|k \subset \text{part } i\}} \tilde{vp}_{k,i}^{(q)}, \quad \text{in which } \tilde{vp}_{k,i}^{(q)} = \mathbf{A}_i^{(q)} \tilde{\mathbf{k}}_i^{(q)}, \quad (8)$$

300 where $\tilde{\mathbf{k}}_i^{(q)}$ is the regularized keypoints¹ location in part i of the q^{th} entire upper
 301 body candidate. $\tilde{vp}_{k,i}^{(q)}$ is the displacements of the keypoints k in part i of the q^{th}
 302 global candidate according to the optical flow. $N_k = 1$ if the keypoint k belongs
 303 to only one part (e.g. head and belly button); otherwise $N_k = 2$ (e.g. shoulder
 304 and elbow), as illustrated in Fig. 2.

305 In addition to the propagated candidates from the previous frame, in order
 306 to improve accuracy in estimating the torso and head locations, we use the FMP
 307 method [10] to add a few additional candidates to the propagated candidates,
 308 as shown in Fig. 4 step2.

309 4.3. Local Layer Pose Estimation

310 After generating a set of global upper body pose candidates, we need to
 311 decompose them into local layer parts, in order to refine each part separately.
 312 Each local layer candidate acquires a scale $s_i^{(j)}$ from the *scale* of the related
 313 global layer candidate. We refine each local layer part in the same sequence as
 314 defined in Eq. (1).

¹ $\tilde{\mathbf{k}}_i^{(q)}$ are used along with the affine matrix $\mathbf{A}_i^{(q)}$ to fit an affine motion model to the optical flow matrix within each body part.

315 A cost function $p(I_{t+1}|\mathcal{C}_i^{(j)})$ is used to evaluate every candidate of each part
 316 in the local layer separately:

$$p(I_{t+1}|\mathcal{C}_i^{(j)}) = \lambda_1 p_{ct}(I_{t+1}|\mathcal{C}_i^{(j)}) + \lambda_2 p_{cl}(I_{t+1}|\mathcal{C}_i^{(j)}) + \lambda_3 p_p(I_{t+1}, I_t|\mathcal{C}_i^{(j)}) \\ + \lambda_4 p_f(I_{t+1}, I_t|\mathcal{C}_i^{(j)}) + \lambda_5 p_h(I_{t+1}, I_t|\mathcal{C}_i^{(j)}). \quad (9)$$

317 The cost function considers five factors. In the first two terms we consider im-
 318 age likelihood, where we use contour $p_{ct}(I_{t+1}|\mathcal{C}_i^{(j)})$ and colour $p_{cl}(I_{t+1}|\mathcal{C}_i^{(j)})$.
 319 The next term is our adaptive penalty $p_p(I_{t+1}, I_t|\mathcal{C}_i^{(j)})$, automatically adapts
 320 constraint terms while estimating limb locations (in contrast to [8] which limits
 321 joint angles to match the motion range of a particular dataset, or [25] which
 322 imposes a-priori kinematic constraints). The remaining two parts relate to mo-
 323 tion likelihood, which are motion cue $p_f(I_{t+1}, I_t|\mathcal{C}_i^{(j)})$ and hand motion offset
 324 $p_h(I_{t+1}, I_t|\mathcal{C}_i^{(j)})$. Because of the magnitude of the five terms, the selection of
 325 corresponding parameters should be $\lambda_3 < 0 < \lambda_4 < \lambda_5 \leq \lambda_2 < \lambda_1$. Fig. 5
 326 illustrates various scores of different part candidates given by the cost function.
 327 It is evident that the highest score provides the best candidate.



Figure 5: Illustration of the discriminative power of the cost function.

328 4.3.1. Image likelihood

329 Firstly, we describe how to calculate contour likelihood $p_{ct}(I_{t+1}|\mathcal{C}_i^{(j)})$. The
 330 scale of human bodies varies greatly within different video sequences, as shown

331 in Fig. 3(c). To make the contour-based likelihood more robust, similar to [8],
 332 we use a three-level pyramid to apply a histogram of oriented gradients (HOG)
 333 descriptor: at the contour, inside the contour, and outside the contour, in order
 334 to obtain a feature vector $h_i(I_{t+1}|\mathcal{C}_i^{(j)})$. Next, a support vector machine (SVM)
 335 classifier is applied to this feature vector to compute $p_{ct}(I_{t+1}|\mathcal{C}_i^{(j)})$.

$$p_{ct}(I_{t+1}|\mathcal{C}_i^{(j)}) = \frac{1}{1 + \exp(a_i \text{svm}(h_i(I_{t+1}|\mathcal{C}_i^{(j)})) + b_i)}, \quad (10)$$

336 where the function $\text{svm}(\cdot)$ means the output of the SVM, a_i and b_i are scalar
 337 parameters [36]. The SVM is trained on a collected dataset (217 images) with
 338 annotations as shown in [9].

339 Next, the colour histograms $h_c(i)$ previously computed for individual parts
 340 (Sec. 4.1) are now used to generate a colour probability map $M_c(i)$ (considering
 341 self-occlusion) for each part, as illustrated using an instance of a lower arm
 342 part in Fig. 6. We handle the self-occlusion by masking other parts in an order
 343 from lower arms to upper arms, and then to torso and head. We use the first
 344 propagated puppet of frame $t+1$ to handle the self-occlusion, in case that the
 345 masked parts would not influence the evaluation of part i . By checking the value
 346 of each pixel within $\mathcal{C}_i^{(j)}$ in $M_c(i)$, we calculate the mean value of these pixels
 347 as colour-based likelihood $p_{cl}(I_{t+1}|\mathcal{C}_i^{(j)})$.

348 4.3.2. Motion likelihood

349 We compute a motion image F_{t+1} , *i.e.* optical flow from frame t to frame
 350 $t+1$, as shown in Fig. 6. When handling the motion image for each part, we
 351 consider the self-occlusions among parts in a similar way with the method used
 352 in Sec.4.3.1, but we also mask the other parts regions of the puppet from frame
 353 t , because the F_{t+1} is calculated using both frame t and $t+1$.

354 The motion image F_{t+1} is masked for each part candidate, and a flow region
 355 $region_i^{(j)}$ for part i in the j^{th} candidate can be computed. Then, the motion-
 356 based likelihood $p_f(I_{t+1}, I_t|\mathcal{C}_i^{(j)})$ is calculated as the mean value of pixels within
 357 this region.

$$p_f(I_{t+1}, I_t|\mathcal{C}_i^{(j)}) = \frac{1}{N} \sum_{(x,y) \in region_i^{(j)}} F_{t+1}(x, y), \quad (11)$$

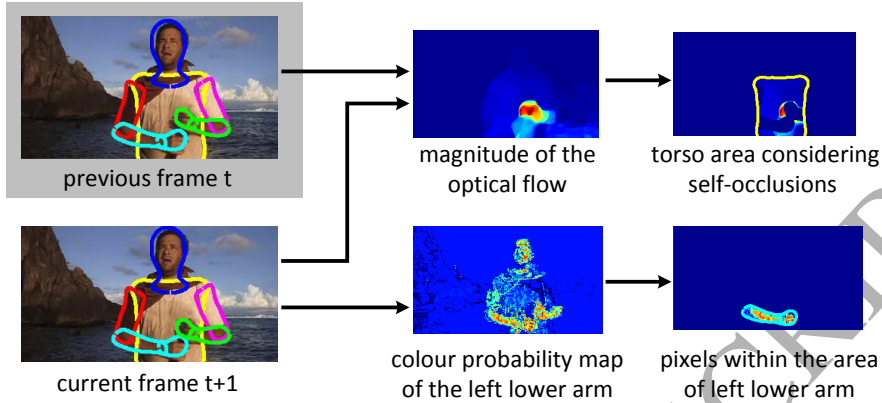


Figure 6: Illustration of the colour probability map and the optical flow magnitude. The images of frame t and $t+1$ are on the left. The **upper middle** image shows the magnitude of the optical flow from frame t to $t+1$, and the **upper right** image shows the magnitude of optical flow for torso area considering self-occlusions. The **lower middle** image reveals the colour probability for the colour of left lower arm area, and the **lower right** image shows the colour probability map pixels within the area of left lower arm.

where, N is the total number of pixels within $region_i^{(j)}$, I_{t+1} and I_t are images corresponding to the frames $t+1$ and t , respectively, and $\mathcal{C}_i^{(j)}$ is the index of the j^{th} local candidate of part i defined in Eq. (3).

Hands (the distal regions of left/right lower arm parts) tend to be more flexible and move faster than other parts, and so should not have the same penalty as other parts. We therefore add the motion-based item only for lower arms ($i \in \{LA_t^r, LA_t^l\}$) to offset some of the penalty. We generate a hand motion map $H_{t+1} = f_h(I_{t+1}, I_t)$ for each frame by using a hand filter [6] over optical flow gradient magnitude. Masking H_{t+1} to get pixels within the hand region $Mask_i^{(j)}$, and the mean value of these pixels is used to build $p_h(I_{t+1}, I_t | \mathcal{C}_i^{(j)})$:

$$p_h(I_{t+1}, I_t | \mathcal{C}_i^{(j)}) = \frac{1}{N} \sum_{(x,y) \in Mask_i^{(j)}} H_{t+1}(x, y). \quad (12)$$

4.3.3. Adaptive penalty

In general, estimating the pose for each part separately may lead to low efficiency and unexpected failures. To overcome this problem, we introduce an

371 adaptive penalty function. We start by computing the displacement value $vp_k^{(q)}$
 372 of each keypoint (denoted by k) in the q^{th} global candidate during propagation
 373 (see Eq.(8)), and record the maximum and minimum values as boundaries. Then
 374 we choose a movement vc_k (between the maximum and minimum) of keypoint
 375 k as:

$$vc_k = \min_{1 \leq q \leq N_q} (vp_k^{(q)}) + \lambda_v (\max_{1 \leq q \leq N_q} (vp_k^{(q)}) - \min_{1 \leq q \leq N_q} (vp_k^{(q)})), \quad (13)$$

376 where, λ_v is a fixed coefficient, and $\lambda_v \in (0, 1)$. We also set keypoint movement
 377 $v_{k,i}^{(j)}$ to be the displacement of k in the j^{th} local candidate of part i from I_t to
 378 I_{t+1} , and the difference between vc_k and $v_{k,i}^{(j)}$ is denoted by $ve_k^{(j)}$. We define the
 379 coarse penalty term as follows:

$$\tilde{p}_p(I_{t+1}, I_t | \mathcal{C}_i^{(j)}) = \sum_{k=\{k|k \subset \text{part } i\}} (\|ve_k^{(j)}\|_2), \quad (14)$$

380 where I_{t+1} and I_t refers to images in frames $t+1$ and t , respectively, and $\mathcal{C}_i^{(j)}$
 381 means the index of the j^{th} local candidate of part i defined in Eq.3.

382 **Human lower arms sometimes move fast, and human body parts frequently**
 383 **self-occlude or may be occluded by other objects.** Consider a situation when a
 384 local part location in frame t is erroneous due to an occlusion, and the occluded
 385 body part re-appears in the next frame. In this case the penalty term in Eq.(14)
 386 may cause problems when the local part needs to correct its pose by rapidly
 387 jumping from the wrong (old) location to the new location of the reappeared
 388 part. Our global layer overcomes this problem.

389 In the global layer, the score, $score_1^{(1)}$ (calculated using Eq.(7)) is recorded
 390 when manually initialising the puppet in the first frame, and $score_{t+1}^{(1)}$ is
 391 calculated after propagating from frame t to frame $t+1$. Additionally, we set a
 392 threshold for penalty as $D_p = \frac{d_c}{2}$, where d_c is defined in Eq.(6). Then revisiting
 393 the local layer, we define our adaptive penalty as follows:

$$p_p(I_{t+1}, I_t | \mathcal{C}_i^{(j)}) = \begin{cases} (\frac{1}{\omega \cdot D_p}) \cdot \tilde{p}_p(I_{t+1}, I_t | \mathcal{C}_i^{(j)}), & \text{if } \tilde{p}_p(I_{t+1}, I_t | \mathcal{C}_i^{(j)}) \leq D_p \\ \frac{1}{\omega} & , \text{ otherwise} \end{cases}, \quad (15)$$

$$\text{where, } \omega = \begin{cases} \frac{\text{score}_1^1 - \text{score}_{t+1}^1}{|\text{score}_1^1|}, & \omega \geq \delta \\ \delta & , \text{ otherwise} \end{cases}, D_p = \frac{d_c}{2}, \delta \text{ is a small positive value}$$

which is set to be 0.1, and $\tilde{p}_p(I_{t+1}, I_t | \mathcal{C}_i^{(j)})$ is the coarse penalty term defined in Eq.(14).

4.4. From Decomposition to Recomposition

After refining local parts, the next step in our method is to recombine all local parts to form a global refined pose. Previously, Yang and Ramanan [10] used a tree model-based method for calculating over all parts iteratively to get the best configuration for the position and type of each root. Later, they generate multiple detections in each image. By tracking the *argmax* indices, they find the location and type of each part in each maximal configuration. Our selection for the best part candidates is different from such methods and is explained below.

As mentioned earlier, we follow the same order mentioned in Eq. (1) for pose computation and now for re-composition we follow the reverse order *i.e.* to calculate from lower arms to torso and head. The hand colour and motion maps can be used to sample the possible wrist locations. However, if the sampled wrist is too far from the elbow (further than the predefined lower arm length threshold), the elbow needs to be relocated to make sure the lengths of both upper and lower arm are within the required range. In this process, we search for a new elbow location along the detected lower arm direction, while ensuring that the lower arm length meets the length constraint. This process also results in new upper arm candidates.

From all the sampled, propagated and initialised results, the cost function defined in Eq.(9) is used to obtain a best set of lower arm candidates \mathbf{N}_{la} . Next, relocated elbows from the previous step result in new upper arm candidates.

From all relocated, propagated and initialised upper arms, the best set of upper arm candidates \mathbf{N}_{ua} are also selected using Eq.(9).

Once we have both upper and lower arm candidates, the next step is to find the complete right and left arms by connecting \mathbf{N}_{ua} and \mathbf{N}_{la} . Each upper and

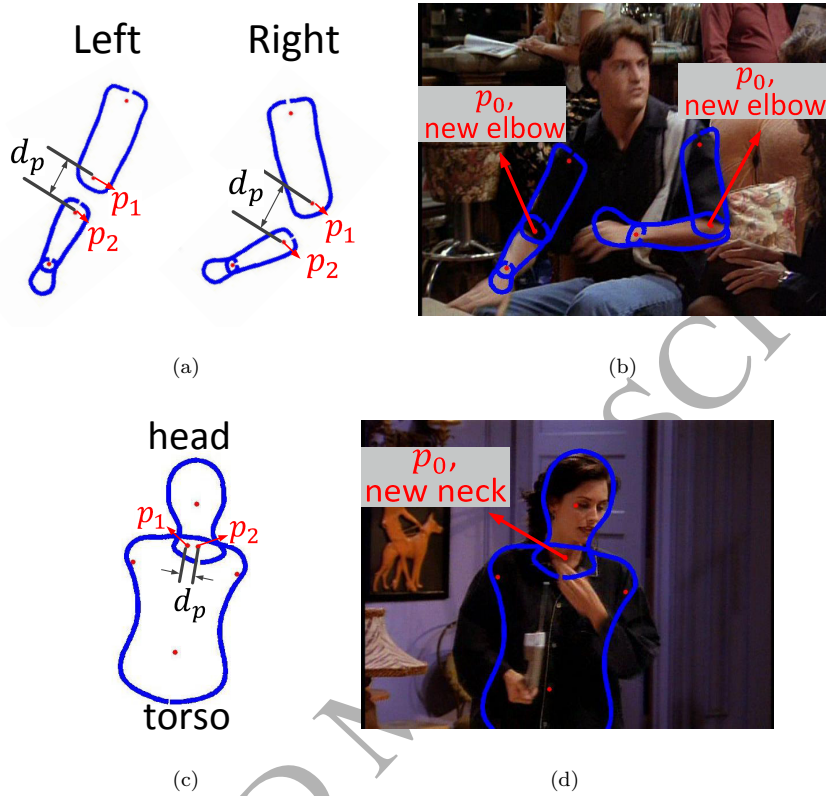


Figure 7: (a) Left and right arm candidates with upper (p_1) and lower (p_2) elbow points. (b) Connected new elbow point p_0 . (c) Head and torso candidates with neck (p_1 and p_2) points. (d) Connected new neck point p_0 .

423 lower arm candidate contains an elbow point (*i.e.* p_1 and p_2 in Fig. 7(a)). The
 424 process is performed in two steps. Initially, the upper and lower arm candidates
 425 are classified into pairs with the smallest Euclidean distance d_p between p_1 and
 426 p_2 to represent various complete arms (Fig. 7(a) shows one pair for left side and
 427 one for right side as examples). In the process of pairing, each half arm (lower
 428 or upper) can be used more than once to ensure every half arm could find its
 429 nearest other half. Secondly, a final elbow location p_0 is obtained using Eq.(16).
 430 The threshold τ in Eq.(16) is used to judge whether or not the two parts are

431 too far away from each other.

$$p_0 = \begin{cases} \frac{p_1 + p_2}{2} & , \text{ if } d_p < \tau \\ p_1 + \frac{1}{10} \cdot d_p & , \text{ otherwise } , \end{cases} \quad (16)$$

432 where, $\tau = \tau_0 \cdot scale$, and τ_0 is a threshold of pixel distance which is set in Table.2
 433 of Sec.5.2.1. p_0 is the new connecting joint point, as illustrated in Fig. 7(b) and
 434 (d).

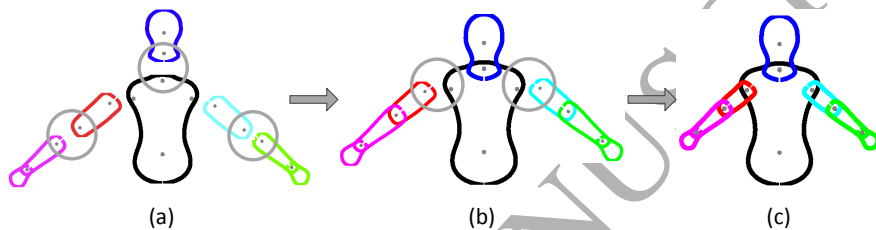


Figure 8: The procedure of connecting local part candidates to obtain a refined global pose.

435 Head and torso pair sets, and torso and left/right upper arm pair sets are
 436 selected in the same way. The procedure for connecting local part candidates
 437 is shown in Fig. 8. In each case the two parts are connected by calculating new
 438 left/right shoulders and new necks, respectively using Eq.(16). When calculating
 439 new necks, the points p_1 , p_2 and p_0 are defined as in Fig. 7(c) and (d); when
 440 calculating new shoulders, p_1 refers to the shoulder point on the torso while p_2
 441 refers to the point on the upper arm, and p_0 refers to the calculated new shoulder
 442 point for the connected torso - upper arm pair. Note that, before calculating
 443 new shoulders, heads are already connected with torsoes and left/right lower
 444 arms are already connected with upper arms, as shown in Fig. 8(b). Once new
 445 shoulders are calculated, the entire bodies are obtained, as shown in Fig 8(c).

446 Next, we return to the global level \mathcal{G}_{t+1} and use Eq.(7) to obtain several best
 447 puppet bodies for propagation to the next frame $t + 2$ (as illustrated in Fig. 4
 448 step1 and discussed in Sec. 4.2). The best global pose candidate is selected as
 449 the final pose for the current frame $t + 1$.

Algorithm 1 Local-Global Coupled-Layer Upper Body Pose Tracker.

-
- 1: Choose \mathcal{K} .
 - 2: Generate global human pose \mathcal{GC} .
 - 3: Perturb \mathcal{GC} to get N_p global candidates.
 - 4: **for** $t = 2, 3, 4, \dots$ **do** $\triangleright t$ means frame index.
 - 5: Propagate N_p \mathcal{GC} s to frame t , and generate N_i \mathcal{GC} s using FMP.
 - 6: Decompose each \mathcal{GC} into P $\mathcal{C}_i^{(j)}$ s. $\triangleright P$ is the number of parts in \mathcal{L}_t .
 - 7: In LA_t^r and LA_t^l , search for new rws and lws , and adjust res and les , which lead to new LA_t^r , LA_t^l , UA_t^r and UA_t^l .
 - 8: **for** $i = 1$ to P **do**
 - 9: Select best $\mathcal{C}_i^{(j)}$ s using Eq.(9).
 - 10: **end for**
 - 11: Make UA_t^r and LA_t^r , UA_t^l and LA_t^l , H_t and T_t into pairs.
 - 12: Connect each pair using p_0 .
 - 13: Connect arms to torsos by calculating p_0 of rsh and lsh , to get \mathcal{GC} s.
 - 14: Select best N_p \mathcal{GC} s using Eq.(7).
 - 15: **end for**
-

450 *4.5. Implementation Analysis*

451 We implement the above presented method in Matlab running on a Win-
452 dows 7 machine with 3.4 GHz Intel i5 CPU. The key steps are summarised in
453 Algorithm.1. Since the method is online, its complexity depends on the number
454 of candidates N and number of parts P to process in the current image. In its
455 current form of implementation, the corresponding asymptotic time complexity
456 is computed to be of $\mathcal{O}(PN)$, where $N = N_p + N_i$. Currently, it takes 4 seconds
457 to process an image and estimate the pose.

458 **5. Experiments**459 *5.1. Datasets Description and Evaluation Methodology*

460 Three different public benchmark datasets have been used for evaluation
461 experiments. The *VideoPose2.0-training* dataset (we didn't use this dataset for

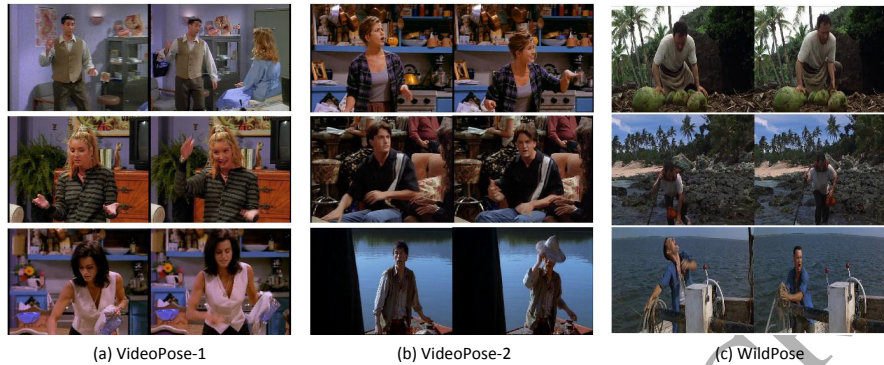


Figure 9: Sample frames of our experimental datasets. (a) Frames from *VideoPose2.0-training* dataset, (b) frames from *VideoPose2.0-testing* dataset, and (c) frames from *Pose in the Wild* dataset.

462 training - only for testing) and *VideoPose2.0-testing* dataset, which contain 26
 463 clips and 18 clips respectively (each clip has about 30 frames), are obtained
 464 from two popular TV series “Friends” and “Lost” [6]. Our experiments use
 465 all sequences of the *VideoPose2.0-training* dataset, referred to as *VideoPose-*
 466 *1*, see Fig. 9(a), and *VideoPose2.0-testing* dataset, referred to as *VideoPose-2*,
 467 see Fig. 9(b). Additionally, we use *Pose in the Wild* dataset [7], a challenging
 468 dataset which has 30 sequences extracted from the Hollywood movies “Forrest
 469 Gump”, “The Terminal”, and “Cast Away”. Each sequence has about 30 frames
 470 with widely changing or deforming body poses. We refer to this dataset as
 471 *WildPose*, see Fig. 9(c).

472 Some well known work, such as [7], evaluate and report their results by
 473 recording the percentage of keypoints that lie within a threshold number of pixels
 474 $error_o$ from the ground truth. However human images in different video
 475 sequences have different scales, which makes it unfair and unmeaningful to
 476 use a constant number of pixels to evaluate the estimation error, as shown in
 477 Fig. 10(a). Therefore, similar to the other SOA methods e.g. [8], we introduce
 478 a normalized set of threshold number of pixels (*pixels error*) $error_r$ as follows:

$$error_r = error_o \times scale, \quad (17)$$



(a) a set of threshold numbers of pixels



(b) a set of normalized threshold numbers of pixels, calculated by Eq.(17)

Figure 10: Un-normalized and normalized threshold number of pixels. Six circles stand for six thresholds, from inside to outside which has 15, 20, 25, 30, 35, 40 pixels radius, respectively. (a) Un-normalized thresholds are too small for the left (large scale) figure but too large for the right (small scale) figure. (b) Normalized thresholds are much more meaningful for frames of different scales.

479 where, $scale$ is illustrated by Fig. 3 in Sec. 3.2. This yields more meaningful eval-
 480 uation results, as demonstrated in Fig. 10(b). For each frame in every sequence,
 481 the $scale$ in Eq.(17) is stored with the ground truth for repeating experiments,
 482 and each method reported in Fig. 11 is evaluated in the same way using Eq.(17).
 483 Fig. 11 plots the elbow and wrist accuracy of each method, averaged over all
 484 frames of all sequences of the respective dataset. The reported elbow/wrist
 485 accuracy is the mean accuracy value of the left and right elbow/wrist. The
 486 horizontal axis in Fig. 11 is the pixels error $error_o$ used in Eq.(17).

487 5.2. Discussion of Human Pose Estimation Results

488 In this subsection, we first compare two variants of our method (*i.e.* with
 489 and without the adaptive penalty term) against four SOA methods, as described

490 in Sec. 5.2.1. Then in Sec. 5.2.2, we evaluate the robustness of our proposed
491 method.

492 5.2.1. Comparison experiments

493 Here we present an experimental evaluation of our coupled-layer method
494 where we compare two different versions of our method against the SOA methods
495 of Zuffi *et al.* [8], Sapp *et al.* [6], Cherian *et al.* [7], as well as Park and Ramanan
496 [15]. The adaptive motion penalty is a critical part of our proposed method. To
497 demonstrate its significance, two different runs are performed with each dataset:
498 one with the penalty and the other without.

499 To perform these comparisons, we used the source code provided by Zuffi *et*
500 *al.* [8] and Cherian *et al.* [7] for their methods to carry out the experiments on
501 all datasets. When using the same datasets as used in the comparison papers,
502 we use parameters as reported by the authors; while for different datasets, we
503 used modified parameters that are chosen using the same methodology proposed
504 by the corresponding work. For the methods of Sapp *et al.* [6] and Park and
505 Ramanan [15], due to the lack of access to their source code, we compare our
506 method against their previously published results with the same public datasets.

507 Note that these comparisons are non-trivial. The problem of “detecting”
508 a human (and its pose) in a single image, is a separate and distinct computer
509 vision problem to that of sequentially tracking a human from one frame to the
510 next. However, many published studies combine both these computer vision
511 problems/methods in a single work, so that the two techniques (detection and
512 tracking) can become confounding factors for evaluating the performance of
513 either. The compared methods are not “online” in that they apply a moderately
514 weak (noisy) pose detector to all frames over an entire video sequence, and then
515 mutually optimise the poses, backwards and forwards, across all frames to satisfy
516 smoothness and mutual compatibility constraints. In contrast, our method is
517 “online” in the sense that it only makes use of information from the preceding
518 frame, to estimate the pose in the current frame. Since our method relies on
519 no prior knowledge except the estimated pose at the previous frame, it would

520 not be fair or meaningful to initialise using a weak or noisy pose detector at
521 the first frame, and we therefore hand-initialise our tracker in the first frame.
522 To ensure a persuasive comparison, we use the same hand-initialised poses in
523 the first frame of each sequence when we evaluate the methods of Zuffi *et al.* [8]
524 and Cherian *et al.* [7] (the results are shown in Fig. 11). We suggest that the
525 compared methods represent the best of the available SOA methods for human
526 pose estimation in video sequences, and it is therefore useful and sensible to
527 show comparison of these “offline” methods against our own “online” method
528 in this paper. We believe that our use of identical hand-initialised poses for the
529 first frame of all compared methods, makes for a fair comparison. Additionally,
530 we note that: i) we have observed that the use (or not) of hand-initialised
531 ground-truth for the first frame of the compared techniques makes very little
532 difference to their performance (unsurprising, since the compared methods rely
533 on separate detections in all frames); ii) in the next section we investigate the
534 sensitivity of our proposed method to varying levels of noise in the initial pose
535 estimate, and find it to be relatively robust against such perturbations.

536 The first row in Fig. 11 shows the experimental results of all methods tested
537 on the *VideoPose2.0-training* dataset. Results of Fig. 11(a) suggest that the pro-
538 posed coupled-layer method with adaptive penalty provides significantly better
539 elbow localization accuracy than [7] and [8], by 16% and 18% respectively at 15
540 *pixels error*, and this superiority is maintained until 40 *pixels error*. Fig. 11(b)
541 shows that the wrist accuracy of our method is around 20% better than [7] and
542 [8] over all *pixels error* thresholds. One possible explanation for the lower per-
543 formance of Zuffi *et al.* [8] on this dataset, is that they assume the lower arm to
544 be of skin colour, *e.g.* people wear semi-sleeve shirts. However only 54% clips
545 in this dataset comply with this condition. Cherian *et al.* [7] have high require-
546 ments of the candidates, but the method they used to obtain pose candidates
547 requires that some frames in the video sequences provide easy to detect poses.
548 In the *VideoPose2.0-training* dataset, people sometimes wear loose clothes with
549 long sleeves and self occlusion often occurs, which limits the accuracy of pose
550 candidates and could be a possible factor to explain the lower accuracy of [7].

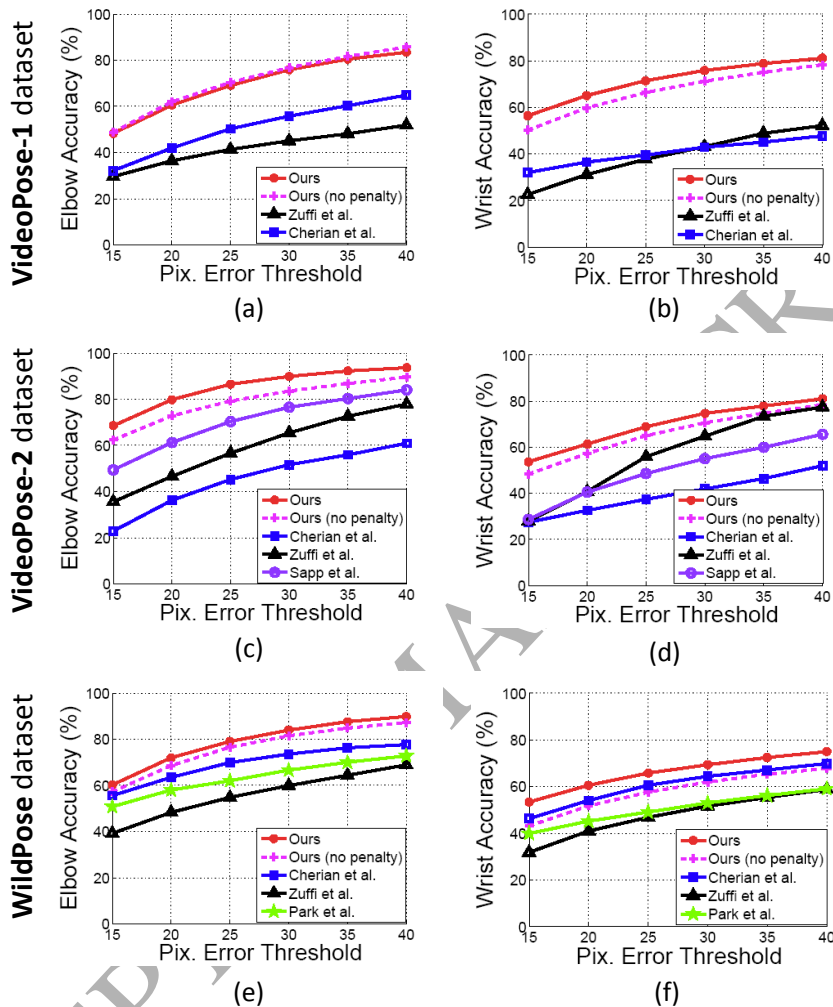


Figure 11: Performance comparison of the proposed method, with and without adaptive penalty, versus other SOA methods.

551 Fig 11(c) shows that our method clearly outperforms the SOA work of [8, 6]
 552 and [7] on elbow accuracy tested on the *VideoPose2.0-testing* dataset. From
 553 Fig. 11(d) we can see that performance accuracy is better than [8, 6, 7] by more
 554 than 20% at 15 pixels error. Then as pixels error is increased, Zuffi *et al.* method
 555 [8] improves comparatively. This is mainly due to the fact that all the poses are

556 iteratively propagated and refined (forwards and backwards) within the entire
 557 video sequence, even if this results in losing the correct pose in many frames.
 558 However, this is the major advantage of our method, where a misjudged wrist
 559 pose in one frame can be corrected directly in the next frame using the proposed
 560 adaptive penalty.

561 The *WildPose* dataset is very different from the *VideoPose2.0* dataset. It
 562 contains more difficult outdoor scenes, with cluttered backgrounds, larger and
 563 faster movements of the tracked person, and rapid camera motion. The hu-
 564 man poses are closer to those of real world scenarios. Our proposed method,
 565 with adaptive penalty term, significantly outperforms the comparison methods
 566 [7, 15] and [8] at all *pixels error* tolerances, on both elbow and wrist metrics, as
 567 presented in Fig. 11(e) and (f). This suggests that such offline learning-based
 568 methods, requiring the entire video sequence to be mutually refined over all
 569 poses in all frames, perform poorly in these challenging conditions compared to
 570 the more highly constrained conditions of the *VideoPose2.0* data. The perfor-
 571 mance of [8] is especially poor, likely due to their use of stronger assumptions
 572 and constraints (*e.g.* upper arm and torso should be of similar colour).

Table 1: Comparison of shoulder accuracy data

Datasets and Methods		Shoulder accuracy at x <i>pixels error</i> (%)					
		x=15	x=20	x=25	x=30	x=35	x=40
<i>VideoPose-1</i>	ours	65.9	79.6	87.6	91.5	93.2	94.0
	[8]	22.8	35.8	48.5	61.6	68.3	72.1
	[7]	63.8	68.6	71.2	72.6	73.8	74.9
<i>VideoPose-2</i>	ours	69.2	82.2	88.8	91.4	93.4	95.0
	[8]	30.4	58.9	79.1	90.1	95.8	96.5
	[7]	63.7	72.1	75.5	77.5	78.3	79.1
<i>WildPose</i>	ours	56.0	71.0	81.5	87.7	91.1	93.4
	[8]	34.9	49.9	63.7	74.2	79.7	84.0
	[7]	66.3	76.1	79.9	81.8	83.5	84.7

573 Torso locations are most likely to represent overall human position, which
 574 is, in turn, the foundation for estimating articulated human pose. Here we
 575 also compare our shoulder accuracy (see Table.1) with the SOA methods of [8]
 576 and [7]. Table.1 reveals that our method significantly outperforms other SOA
 577 methods in terms of accuracy of torsos.

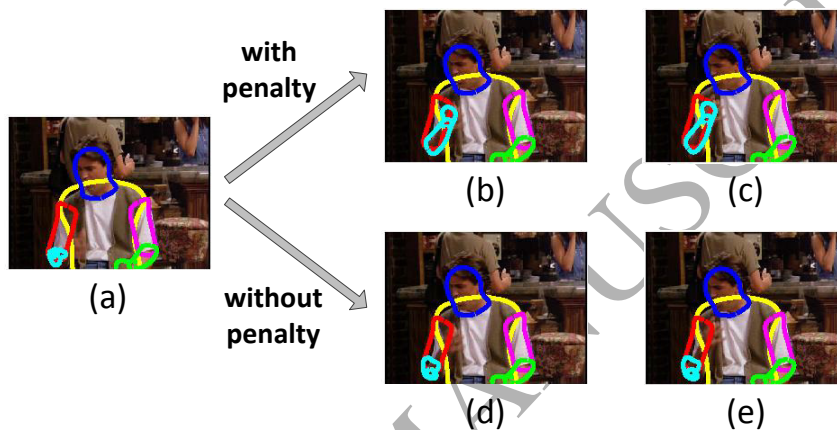


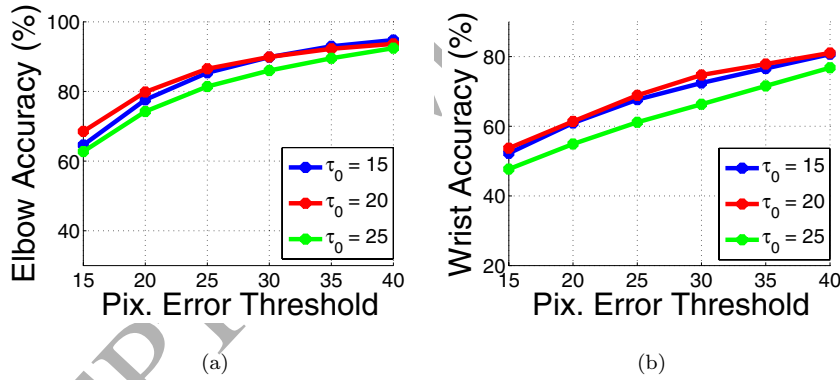
Figure 12: Performance analysis of using adaptive penalty. From the same frame with pose (a), poses (b) and (c) are achieved with penalty term, while poses (d) and (e) are achieved without penalty term. It can be clearly seen that the estimation performance is better using the penalty term.

578 Additionally, note that the advantage of using the adaptive penalty term
 579 with our coupled-layer method is clearly noticeable in all experiments of Fig. 11.
 580 Fig. 12 shows some examples to illustrate how the adaptive penalty term is able
 581 to improve pose tracking accuracy.

582 The parameter values used to test the method and their corresponding se-
 583 lection criteria are summarized in Table.2. Among these parameters, only τ_0 in
 584 Eq.(16) has been hand selected (constant) for the sake of implementation con-
 585 venience. However, we vary its value and test our method on the *VideoPose2.0-*
 586 *testing* dataset in order to find the sensitivity of method to τ_0 . Fig. 13 illustrates
 587 the resulting tracking accuracy for various τ_0 values. These results demonstrate
 588 that our proposed method is not sensitive to varying the value of τ_0 . The values

Table 2: List of the parameters used in the experiments and corresponding selection criteria.

Equation	Coefficients	Selection
global candidates score Eq.(7)	$\lambda_\psi=1, \lambda_\phi=0.03$	$\lambda_\psi \gg \lambda_\phi$
local part candidates score Eq.(9)	$\lambda_1=4, \lambda_2=1, \lambda_3=-0.6,$ $\lambda_4=0.5, \lambda_5=1$	$\lambda_4 < \lambda_5 \leq \lambda_2 < \lambda_1,$ $\{\lambda_1, \lambda_2, \lambda_4, \lambda_5\} \in R_{>0},$ $\lambda_3 \in R_{<0}$
global layer keypoint movement Eq.(13)	$\lambda_v=2/3$	$0 < \lambda_v < 1$
relocate new keypoint Eq.(16)	$\tau_0=20.$	$\tau_0 < 25,$ not sensitive, see Fig. 13

Figure 13: Proposed method is not sensitive to varying values of τ_0 . (a) elbow accuracy when varying τ_0 ; (b) wrist accuracy while varying τ_0 .

589 of the parameters reported in Table.2 are fixed for all our experiments *i.e.*, for
590 all the sequences of all three datasets.

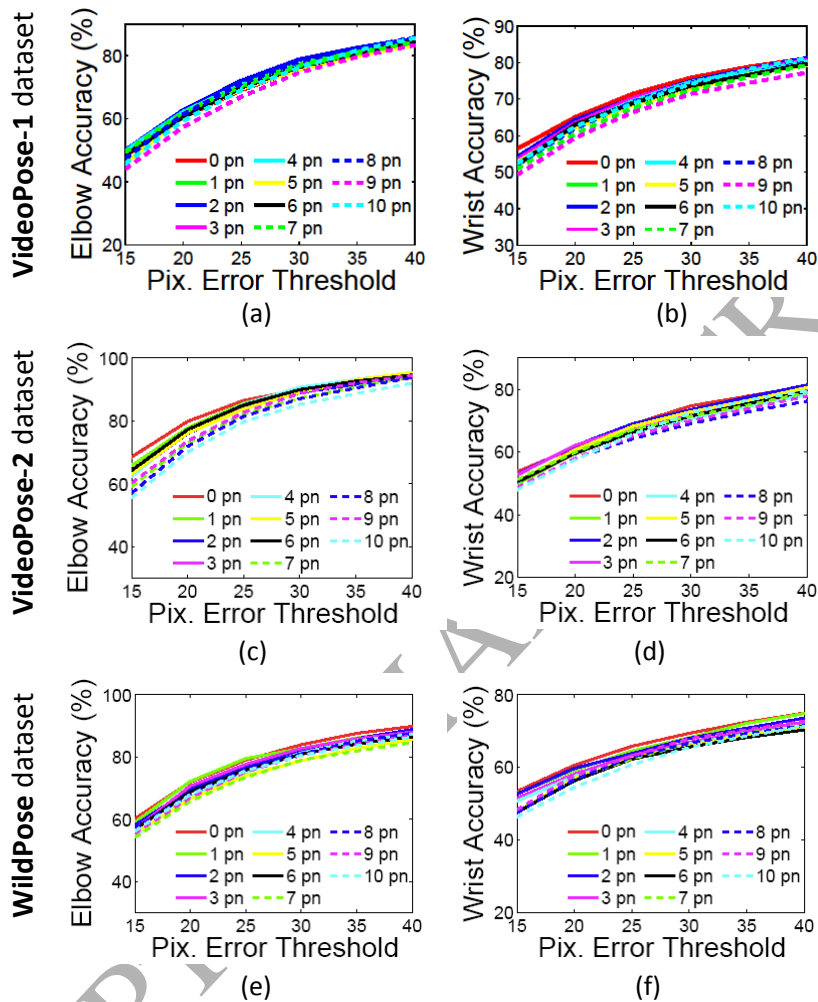


Figure 14: Results of using Gaussian noise to perturb the hand-initialised pose for the first frame of every video sequence. The amplitude of Gaussian noise ranges from 1 to 10 pixels. The unit 'pn' in legend means *pixel noise*, which refers to the amplitude of Gaussian noise.

5.2.2. Robustness experiments

To investigate the robustness of our method to varying levels of noise in the initial pose estimates at the first frame, we add noise to perturb these manually initialised poses, and use these perturbed poses to initialise our method. We perturb the ground-truth (manually initialised) poses by applying Gaussian

Table 3: Robustness for Initialization

Datasets and Joint Points		Accuracy with n pixels amplitude				
		Gaussian noise (%)				
		$n=0$	$n=4$	$n=7$	$n=10$	<i>average</i>
<i>VideoPose-1</i>	<i>sh</i>	91.5	91.0	90.6	89.2	90.5
	<i>el</i>	75.9	76.5	76.8	76.0	76.7
	<i>wr</i>	75.8	74.6	72.4	74.2	74.0
<i>VideoPose-2</i>	<i>sh</i>	91.4	92.3	92.0	92.3	92.2
	<i>el</i>	89.9	90.7	87.2	85.3	88.7
	<i>wr</i>	74.7	71.0	71.4	72.5	72.2
<i>WildPose</i>	<i>sh</i>	87.7	86.8	85.6	85.3	85.6
	<i>el</i>	83.0	81.3	79.0	80.5	81.0
	<i>wr</i>	69.4	68.0	66.7	65.6	67.1

In this table, *sh* means *shoulders*, *el* means *elbows*, and *wr* means *wrists*. *average* means the average accuracy value among n ranges from 1 to 10.

596 noise, with amplitudes varying from 1 pixel to 10 pixels. We perturb the first
 597 frame pose for *VideoPose2.0-testing* dataset, *VideoPose2.0-testing* dataset and
 598 *Pose in the Wild* dataset separately. Fig. 14 shows the accuracy results for both
 599 elbow and wrist of each dataset, and Table.3 shows instance accuracy of shoul-
 600 ders, elbows and wrist for different amplitudes of Gaussian noise at 30 *pixels*
 601 *error*. The average accuracy of joint points among adding Gaussian noise from
 602 1 to 10 pixels is also shown in Table.3. It can be seen that the added noise in
 603 the initial frame does not noticeably affect performance. This suggests that our
 604 method is robust to noisy initial pose estimates in the first frame. This phe-
 605 nomenon further supports the validity of the previous section which compares
 606 the performance of our tracker against SOA methods which rely on separate
 607 detections at each frame (see previous discussion of this).

608 Furthermore, we also demonstrate our method using the automatic initial-
 609 ization technique shown in [10]. We perform this test using the *VideoPose2.0-*

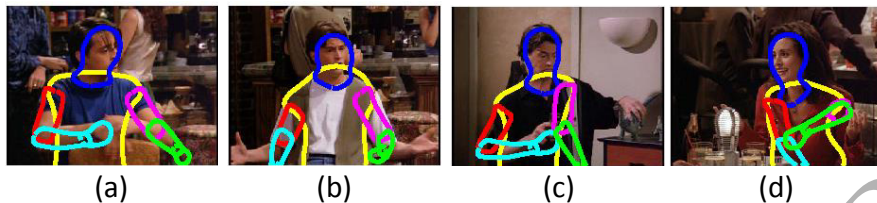
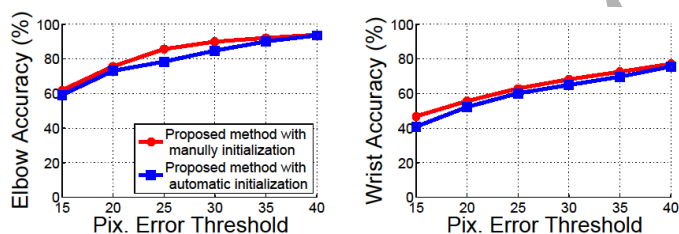
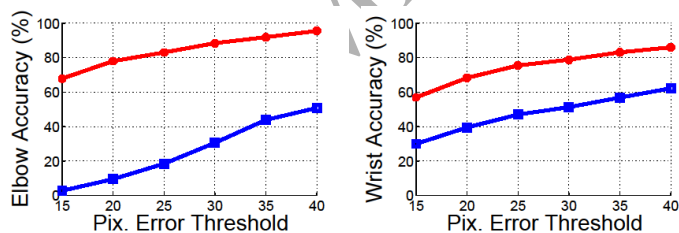


Figure 15: Samples of automatic initialization in the first frame. (a) and (b) show samples of acceptable auto-initialization; (c) and (d) show wrong auto-initialization, which cannot give correct information to the system.



(a) Implemented with acceptable automatic initializations



(b) Implemented with bad automatic initializations

Figure 16: Results of our proposed method with automatic initialization in the first frame. (a) shows result obtained by implementing with acceptable auto-initialization; (b) shows result obtained by implementing with wrong auto-initialization.

610 *testing* dataset, where the human body pose in the first frame has been auto-
 611 matically initialised. The dataset contains 18 clips, out of which the automatic
 612 initialization was acceptably successful for 12 clips and performed poorly for
 613 the rest, as shown in Fig. 15. Obtained accuracies in both cases are shown in
 614 Fig. 16. As expected, the results show that the proposed pose tracker works

615 reasonably well in the case of effective initialization. In contrast, in cases where
 616 the automatic initialization failed, then successive tracking has difficulty in re-
 617 covering from the very large initial errors. This is due to the fact that the
 618 proposed method does not rely on any prior knowledge, while the automatic
 619 initialization fails to give correct target information.

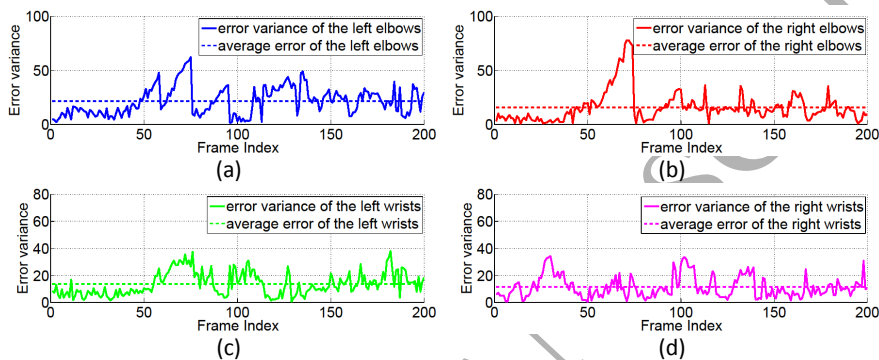


Figure 17: Pose error variance and average error of the joints of left/right elbows and left/right wrists.

620 Additionally, we also test our proposed method on a video file containing 200
 621 frames to check the existence of drift while tracking. The pose error variance
 622 has been computed over entire sequence and is shown in Fig. 17. The obtained
 623 results clearly suggest that the error does not accumulate over time and hence,
 624 the method does not suffer from drift. Moreover, it is evident that the method
 625 is able to robustly converge on good poses in new frames following large errors
 626 in previous frames.

627 5.3. Visual Comparisons of Performance

628 Fig. 18 shows example visualisations of our method’s results in comparison
 629 with the methods of [7] and [8] testing on the *VideoPose2.0-training* dataset,
 630 while Fig. 19 shows results for the *VideoPose2.0-testing* dataset. Fig. 20 shows
 631 results for the *Pose in the Wild* dataset. To compare with [7], we use the
 632 keypoints of our *coupled-layer DS puppet model* to draw stick poses, in order

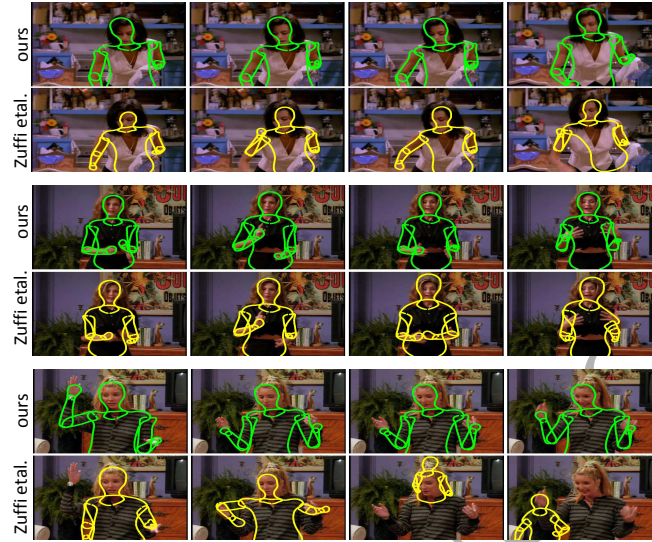
633 that poses are presented in the same way as [7]. In each comparison pair set,
 634 the first row represents the results of our method and the second row shows
 635 results for the comparison methods. Several instances can be seen where our
 636 method correctly estimates a pose while [7] and [8] generate substantial pose
 637 errors. Also check the provided supplementary video for better understanding
 638 of the results.

639 The second row of the first pair set in Fig. 18(a) shows that the person's lower
 640 arm jumps to a poor pose estimate (second and fourth columns), this problem
 641 is caused by a higher image likelihood of colour and contour when using Zuffi
 642 *et al.*'s method. In contrast, our proposed method overcomes this problem by
 643 exploiting an adaptive penalty term. The second row of the third pair set in
 644 Fig. 18(a) shows significant errors and erratic pose changes for Zuffi *et al.*. This
 645 is likely caused by the method of Zuffi *et al.* using a cost function for the entire
 646 body to evaluate each pose. In contrast, our proposed method evaluates the pose
 647 of each body part separately and then connects them according to a distance
 648 rule, which makes the resulting pose estimate more robust. The inaccuracy of
 649 Zuffi *et al.* in the second row of the third pair set in Fig. 19(a) is caused by
 650 the assumption that lower arms, in addition to hands, are always skin coloured.
 651 The second pair set in Fig. 20(a) illustrates the superiority of our method in
 652 calculating scale. When humans move from far to near ranges, our proposed
 653 method can robustly detect the scale change, whereas the method of [8] cannot.

654 The method of Cherian *et al.* requires a large quantity of human pose candi-
 655 dates, and then uses the the entire video sequence to mutually refine them. This
 656 method is able to improve the overall estimation accuracy level, but sacrifices
 657 making full use of the image likelihood of each frame.

658 6. Conclusion

659 We have proposed a novel coupled-layer method for online human pose track-
 660 ing, which demonstrates state-of-the-art adaptability, precision and robustness
 661 over a variety of video sequences. Global holistic models struggle to handle the

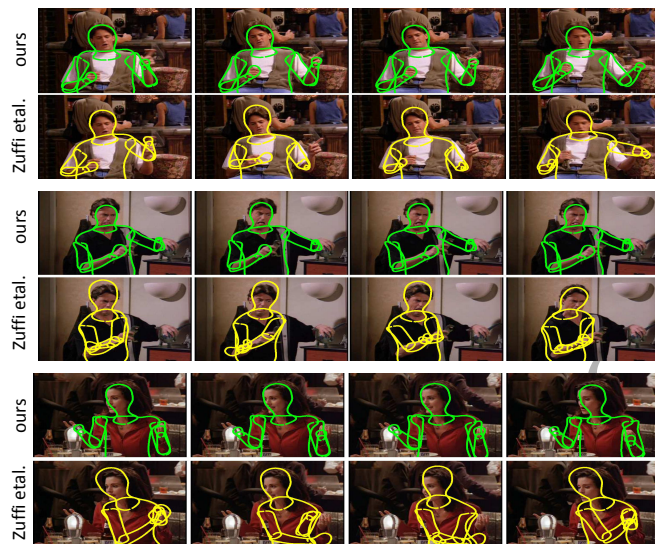


(a)

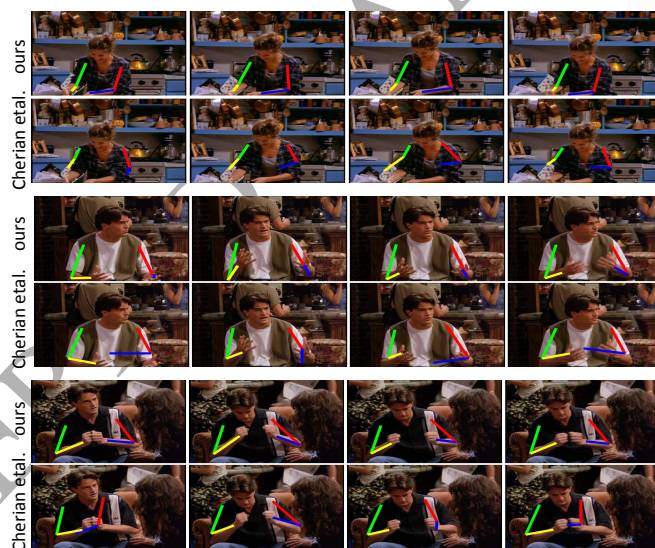


(b)

Figure 18: Example images comparing our results (using adaptive penalty) with the methods of Zuffi *et al.* [8] (sub-figure(a)) and Cherian *et al.* [7] (sub-figure(b)) on *VideoPose2.0-training* dataset. Each sub-figure has three pair sets, and in each pair set, the first row reveals sample results of our method, and the second row reveals the compared method.

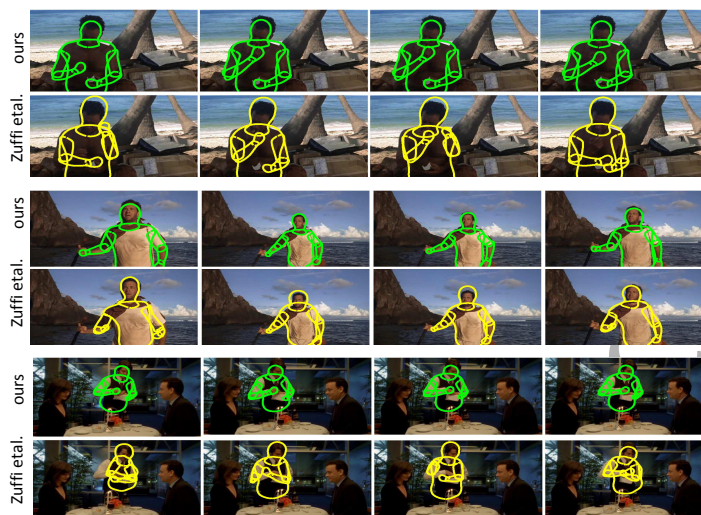


(a)

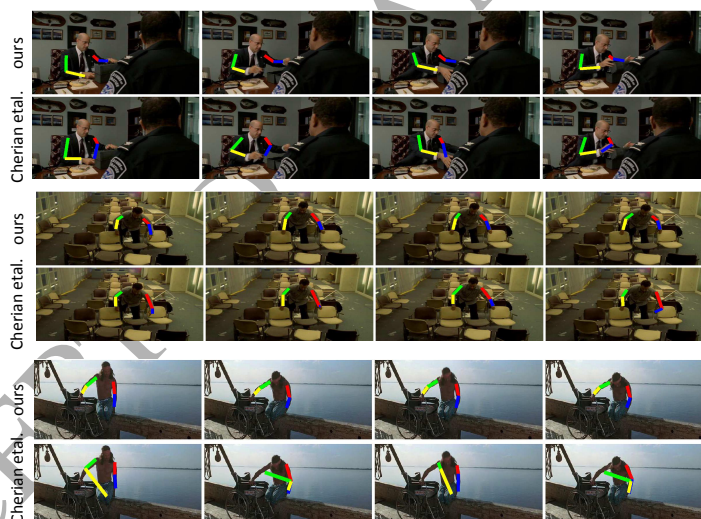


(b)

Figure 19: Sample results compared our results (using adaptive penalty) with the methods of Zuffi *et al.* [8] (sub-figure(a)) and Cherian *et al.* [7] (sub-figure(b)) on *VideoPose2.0-testing* dataset. Each sub-figure has three pair sets, and in each pair set, the first row reveals sample results of our method, and the second row reveals the compared method.



(a)



(b)

Figure 20: Sample results comparing our method (using adaptive penalty) with the methods of Zuffi *et al.* [8] (sub-figure(a)) and Cherian *et al.* [7] (sub-figure(b)) on *Pose in the Wild* dataset. Each sub-figure has three pair sets, and in each pair set, the first row reveals sample results of our method, and the second row reveals the compared method.

662 complexity of highly articulated objects, whereas parts-based methods lead to
663 pose errors if not sufficiently constrained. Our coupled layer model combines
664 elements of each approach to outperform previous methods. We also incorpo-
665 rated an adaptive motion penalty which can correct the pose of a human body
666 part which has drifted from the previous frame. Our method relies only on the
667 present and previous frames (except the first frame), and so is suitable for online
668 sequential tracking. However, it still outperforms offline methods which rely on
669 mutually optimising poses at all frames over the entire video sequence.

670 **Acknowledgements**

671 This work was funded in part by a scholarship from Shandong University,
672 China, and has also been supported in part by the Innovate UK KTP part-
673 nership 9573 between the KUKA Robotics UK Ltd. and the University of
674 Birmingham.

675 Authors would like to thank Dr. Silvia Zuffi and Dr. Anoop Cherian for
676 making their code publicly available, and for providing us with valuable help
677 and advice for validating and comparing our proposed method.

678 **References**

- 679 [1] D. Hogg, Model-based vision: a program to see a walking person, *Image*
680 *and Vision Computing*. 1 (1) (1983) 5–20.
- 681 [2] A. Yao, J. Gall, G. Fanelli, L. J. Van Gool, Does human action recognition
682 benefit from pose estimation, in: *Proceedings of the British Machine Vision*
683 *Conference*. BMVC Press, Vol. 3, 2011, p. 6.
- 684 [3] X. P. Burgos-Artizzu, P. Dollár, D. Lin, D. J. Anderson, P. Perona, So-
685 cial behavior recognition in continuous video, in: *Conference on Computer*
686 *Vision and Pattern Recognition (CVPR)*, IEEE, 2012, pp. 1322–1329.

- 687 [4] J. Charles, T. Pfister, D. Magee, D. Hogg, A. Zisserman, Domain adapta-
688 tion for upper body pose tracking in signed tv broadcasts, in: Proceedings
689 of the British Machine Vision Conference. BMVC Press, 2013.
- 690 [5] P. Agarwal, S. Kumar, J. Ryde, J. J. Corso, V. N. Krovi, Estimating hu-
691 man dynamics on-the-fly using monocular video for pose estimation, in:
692 Robotics: Science and Systems, Citeseer, 2012.
- 693 [6] B. Sapp, D. Weiss, B. Taskar, Parsing human motion with stretchable mod-
694 els, in: Conference on Computer Vision and Pattern Recognition (CVPR),
695 IEEE, 2011, pp. 1281–1288.
- 696 [7] A. Cherian, J. Mairal, K. Alahari, C. Schmid, Mixing body-part sequences
697 for human pose estimation, in: Conference on Computer Vision and Pattern
698 Recognition (CVPR), IEEE, 2014, pp. 2361–2368.
- 699 [8] S. Zuffi, J. Romero, C. Schmid, M. J. Black, Estimating human pose with
700 flowing puppets, in: International Conference on Computer Vision (ICCV),
701 IEEE, 2013, pp. 3312–3319.
- 702 [9] S. Zuffi, O. Freifeld, M. J. Black, From pictorial structures to deformable
703 structures, in: Conference on Computer Vision and Pattern Recognition
704 (CVPR), IEEE, 2012, pp. 3546–3553.
- 705 [10] Y. Yang, D. Ramanan, Articulated human detection with flexible mixtures
706 of parts, *IEEE Transactions on Pattern Analysis and Machine Intelligence*
707 (PAMI), 35 (12) (2013) 2878–2890.
- 708 [11] M. Dantone, J. Gall, C. Leistner, L. Van Gool, Human pose estimation
709 using body parts dependent joint regressors, in: Conference on Computer
710 Vision and Pattern Recognition (CVPR), IEEE, 2013, pp. 3041–3048.
- 711 [12] M. A. Fischler, R. A. Elschlager, The representation and matching of pic-
712 torial structures, *IEEE Transactions on Computers*. 22 (1) (1973) 67–92.

- 713 [13] L. Pishchulin, A. Jain, M. Andriluka, T. Thormahlen, B. Schiele, Artic-
714 ulated people detection and pose estimation: Reshaping the future, in:
715 Conference on Computer Vision and Pattern Recognition (CVPR), IEEE,
716 2012, pp. 3178–3185.
- 717 [14] M. Eichner, M. Marin-Jimenez, A. Zisserman, V. Ferrari, 2d articulated
718 human pose estimation and retrieval in (almost) unconstrained still images,
719 International Journal of Computer Vision (IJCV). 99 (2) (2012) 190–214.
- 720 [15] D. Park, D. Ramanan, N-best maximal decoders for part models, in: Inter-
721 national Conference on Computer Vision (ICCV), IEEE, 2011, pp. 2627–
722 2634.
- 723 [16] O. Freifeld, A. Weiss, S. Zuffi, M. J. Black, Contour people: A parameter-
724 ized model of 2d articulated human shape, in: Conference on Computer
725 Vision and Pattern Recognition (CVPR), IEEE, 2010, pp. 639–646.
- 726 [17] Y. Wu, T. S. Huang, Capturing articulated human hand motion: A divide-
727 and-conquer approach, in: International Conference on Computer Vision
728 (ICCV), Vol. 1, IEEE, 1999, pp. 606–611.
- 729 [18] K. Paul, M. Dimitrios, N. Jean-Christophe, Integration of bottom-up/top-
730 down approaches for 2d pose estimation using probabilistic gaussian mod-
731 elling, Computer Vision and Image Understanding (CVIU). 115 (2) (2011)
732 242–255.
- 733 [19] M. W. Lee, R. Nevatia, Human pose tracking using multi-level structured
734 models, in: European Conference on Computer Vision (ECCV), Springer
735 Berlin Heidelberg, 2006, pp. 368–381.
- 736 [20] P. F. Felzenszwalb, D. P. Huttenlocher, Pictorial structures for object recog-
737 nition, International Journal of Computer Vision (IJCV). 61 (1) (2005)
738 55–79.

- 739 [21] D. Ramanan, D. A. Forsyth, A. Zisserman, Strike a pose: Tracking people
740 by finding stylized poses, in: *Computer Vision and Pattern Recognition*
741 (CVPR), Vol. 1, IEEE, 2005, pp. 271–278.
- 742 [22] V. Ferrari, M. Marín-Jiménez, A. Zisserman, 2d human pose estimation
743 in tv shows, in: *Statistical and Geometrical Approaches to Visual Motion*
744 *Analysis*, Springer, 2009, pp. 128–147.
- 745 [23] L. Sigal, M. J. Black, Measure locally, reason globally: Occlusion-sensitive
746 articulated pose estimation, in: *Computer Vision and Pattern Recognition*
747 (CVPR), Vol. 2, IEEE, 2006, pp. 2041–2048.
- 748 [24] V. I. Morariu, D. Harwood, L. S. Davis, Tracking people’s hands and feet
749 using mixed network and/or search, *IEEE Transactions on Pattern Analysis*
750 *and Machine Intelligence (PAMI)*. 35 (5) (2013) 1248–1262.
- 751 [25] K. Fragkiadaki, H. Hu, J. Shi, Pose from flow and flow from pose, in:
752 *Conference on Computer Vision and Pattern Recognition (CVPR)*, IEEE,
753 2013, pp. 2059–2066.
- 754 [26] N. G. Cho, A. L. Yuille, S. W. Lee, Adaptive occlusion state estimation
755 for human pose tracking under self-occlusions, *Pattern Recognition* 46 (3)
756 (2013) 649–661.
- 757 [27] X. Chen, A. L. Yuille, Articulated pose estimation by a graphical model
758 with image dependent pairwise relations, in: *Advances in Neural Informa-*
759 *tion Processing Systems(NIPS)*, 2014, pp. 1736–1744.
- 760 [28] L. Sigal, M. J. Black, Predicting 3d people from 2d pictures, *Articulated*
761 *Motion and Deformable Objects*. (2006) 185–195.
- 762 [29] Y. Yang, D. Ramanan, Articulated pose estimation with flexible mixtures-
763 of-parts, in: *Computer Vision and Pattern Recognition (CVPR)*, IEEE,
764 2011, pp. 1385–1392.

- 765 [30] X. Burgos-Artizzu, D. Hall, P. Perona, P. Dollár, Merging pose estimates
766 across space and time, in: Proceedings of the British Machine Vision Con-
767 ference. BMVC Press, Citeseer, 2013.
- 768 [31] D. Anguelov, P. Srinivasan, D. Koller, S. Thrun, J. Rodgers, J. Davis,
769 Scape: shape completion and animation of people, in: ACM Transactions
770 on Graphics (TOG), Vol. 24, ACM, 2005, pp. 408–416.
- 771 [32] L. Cehovin, M. Kristan, A. Leonardis, Robust visual tracking using an
772 adaptive coupled-layer visual model, IEEE Transactions on Pattern Anal-
773 ysis and Machine Intelligence (PAMI). 35 (4) (2013) 941–953.
- 774 [33] S. J. Pan, Q. Yang, A survey on transfer learning., IEEE Transactions on
775 Knowledge and Data Engineering 22 (10) (2010) 1345–1359.
- 776 [34] P. Buehler, M. Everingham, D. P. Huttenlocher, A. Zisserman, Upper body
777 detection and tracking in extended signing sequences, International Journal
778 of Computer Vision (IJCV). 95 (2) (2011) 180–197.
- 779 [35] C. Liu, Beyond pixels: exploring new representations and applications
780 for motion analysis, Ph.D. thesis, Massachusetts Institute of Technology
781 (2009).
- 782 [36] J. Platt, Probabilistic outputs for support vector machines and compar-
783 isons to regularized likelihood methods, Advances in large margin classifiers
784 10 (3) (1999) 61–74.